Ferromagnetic exchange in α-manganese molybdate and the structural consequences

1990 J. Phys.: Condens. Matter 2 6999

(http://iopscience.iop.org/0953-8984/2/33/012)

J. Phys.: Condens. Matter 2 (1990) 6999–7007. Printed in the UK

Ferromagnetic exchange in α-manganese molybdate and the structural consequences

J P Attfield
Chemical Crystallography Laboratory, University of Oxford, 9 Parks Road, Oxford OX1 3PD, UK

Received 6 April 1990

Abstract. Powder neutron diffraction patterns of α-$MnMoO_4$ have been recorded between 2 and 127 K in 0.48 K intervals. A subtle structural transition from $C2/m$ to $P2/m$ (or lower) symmetry is observed at $T_s = 79.1(2)$ K and antiferromagnetic order occurs below $T_N = 10.7(2)$ K. The magnetic structure consists of collinear Mn^{2+} moments of 4.71(3) μ_B close to the [101] direction of the $\boldsymbol{a} \times \boldsymbol{b} \times 2\boldsymbol{c}$ magnetic supercell. The moment reduction due to covalency is compared to that in other oxo salts of d^5 cations. Ferromagnetic alignment of the four spins within Mn_4O_{16} clusters of edge-sharing MnO_6 octahedra is observed and weaker antiferromagnetic interactions between clusters are mediated by molybdate groups. A potential exchange mechanism involving spin transfer from three Mn^{2+} ions onto one O^{2-} is proposed to explain the unusual ferromagnetic interaction. Refinements of the crystal structure using each of the 260 diffraction profiles reveal an exchange-strictive structural distortion around T_N that is consistent with the ferromagnetic interactions within the clusters.

1. Introduction

Anhydrous transition-metal oxo salts exhibit a wide variety of magnetic properties due in part to the many different structures that may be adopted. Such materials often possess simple crystal structures which allows the ordered magnetic and crystal structures to be determined simultaneously using low-temperature powder neutron diffraction. Such methods have previously been used in this laboratory for the study of MXO_4 compounds containing octahedrally coordinated spin-only cations and tetrahedral anions [1–4]. Continuing advances in powder neutron diffractometry and whole profile fitting programs based on the Rietveld method [5] enable many diffraction patterns to be collected in small temperature steps and fitted automatically in sequence. This gives a detailed insight into the changes that accompany a structural [6] or magnetic [7] phase transition. Such an experiment has been performed here to determine the spin arrangement and structural changes in α-$MnMoO_4$ between 2 and 127 K.

Monoclinic α-$MnMoO_4$ ($a = 10.469(5)$ Å, $b = 9.516(5)$ Å, $c = 7.143(5)$ Å, $\beta = 106.3(1)°$ at STP [8]) contains Mn_4O_{16} clusters of four edge-sharing MnO_6 octahedra (figure 1). These clusters have $2/m$ (C_{2h}) symmetry and should give rise to strong magnetic superexchange between Mn^{2+} spins through the shared edges, as indicated in figure 1. Figure 2 shows the linking of clusters by molybdate tetrahedra. The magnetic order in this interesting network has not been determined for α-$MnMoO_4$ or any

0953-8984/90/336999 + 09 $03.50

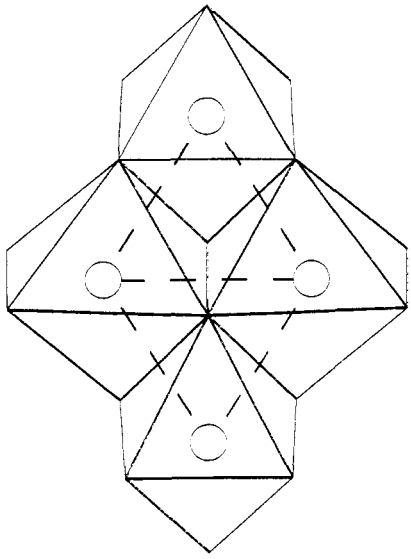

Figure 1. The Mn_4O_{16} cluster in α-$MnMoO_4$, consisting of four edge-sharing MnO_6 octahedra with Mn positions shown as circles and the magnetic interactions indicated by broken lines.

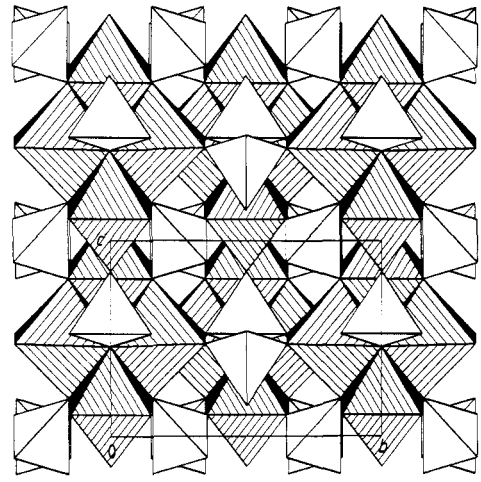

Figure 2. (100) polyhedral projection of the α-$MnMoO_4$ structure with the unit cell marked, showing the clusters of MnO_6 octahedra (shaded) linked by molybdate tetrahedra (unshaded).

isomorph, although a magnetic susceptibility study has revealed an antiferromagnetic transition at 13 K [9].

2. Experimental procedure

10 g of pure, polycrystalline α-$MnMoO_4$ were prepared by firing equimolar amounts of $Mn(CH_3CO_2)_2 \cdot 4H_2O$ and MoO_3 in air at 530 °C for 16 h and then at 700 °C for 45 h.

Neutron diffraction data were collected at the ILL, Grenoble, France. Patterns were recorded between 2 and 127 K on diffractometer D1B at a wavelength of 2.522 Å with a stationary position-sensitive detector covering 2θ = 5–85° in 0.2° steps. The sample was cooled to 2.0 K in a helium cryostat and warmed at 0.16 K min^{-1} while profiles were recorded every 3 min, resulting in 260 patterns in 0.48 K intervals (figure 3). A diffraction pattern was also collected at 50 K on the high-resolution diffractometer D1A between 2θ = 10–150° in 0.05° steps over 8 h at a wavelength of 1.909 Å.

3. Results

The profiles were fitted by modifying a standard program [10] to perform sequential magnetic and nuclear structure refinements. Neutron scattering lengths and a magnetic form factor for Mn^{2+} were taken from standard works [11, 12].

Examination of the D1B profiles in figure 3 reveals a magnetic ordering transition at a Néel Temperature of T_N = 10.7(2) K and a small, previously unknown, structural transition at T_s = 79.1(2) K. Data above T_s were fitted by refining the room temperature

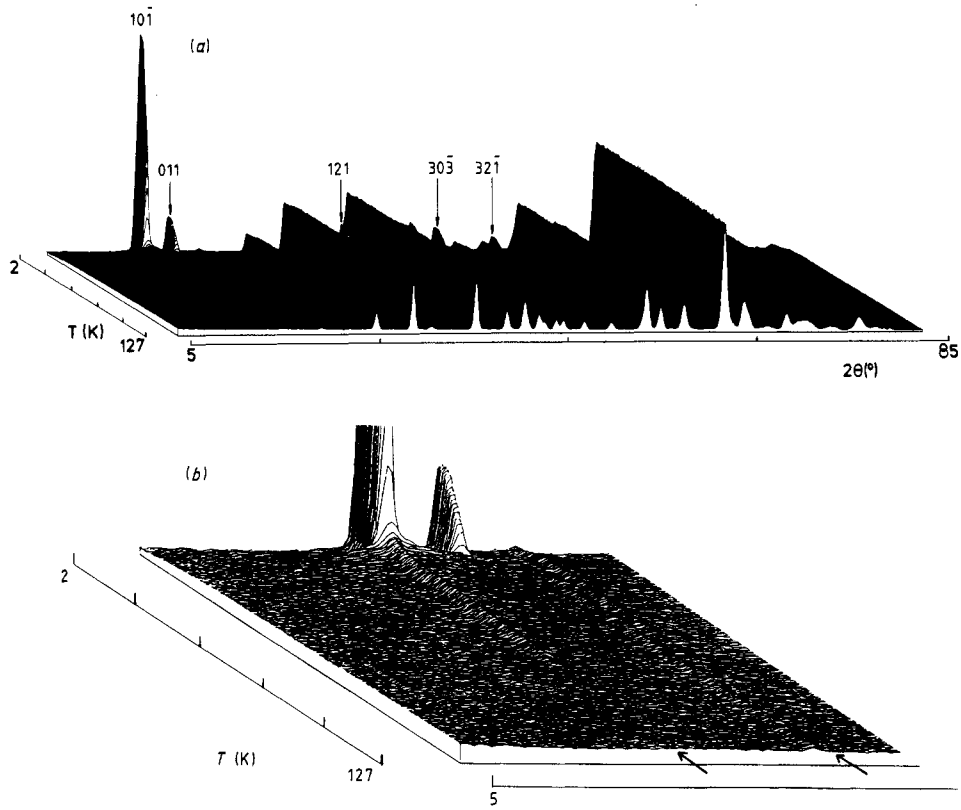

Figure 3. (*a*) Temperature evolution of the neutron diffraction pattern of α-$MnMoO_4$ between 2 and 127 K with prominent magnetic peaks indexed on the magnetic supercell. (*b*) Enlargement of the low-angle region with the two weak peaks that disappear at 79 K arrowed.

structure [8] in space group $C2/m$ (No 12) and the extra peaks observed below this temperature could all be indexed on the same unit cell by lowering the symmetry to $P2/m$. Attempts to refine the structure in this space group using the 50 K D1A data were unsuccessful due to the paucity of observed $h + k = 2n + 1$ reflections, so the profile was fitted in $C2/m$, giving the results shown in tables 1 and 2, and the nuclear parts of all the patterns below T_s were also fitted in this space group. Refining individual, isotropic temperature factors with the 50 K D1A data gave large values for Mo(2), O(2), and O(5), but unrealistic negative values for some other atoms.

Initially, all of the structural parameters were refined independently using each D1B profile. The resulting coordinates were imprecise and gave several unrealistic bond distances and angles, and so the parameters that were not observed to vary significantly with temperature (Mo(1):x; O(1):x; O(2):x; O(3):x, y, z; O(5):x, z) were fixed at the values obtained from the 50 K D1A refinement and the remaining parameters were varied again. This gave atomic positions that were precise to 0.005–0.02 Å and more realistic distances and angles. The temperature dependences of the cell parameters and volumes are shown in figure 4, and the variations in selected bond distances and angles are shown in figures 5 and 6.

Table 1. Results of the refinement of α-$MnMoO_4$ in space group $C2/m$ (No 12) using 50 K D1A powder neutron diffraction data with ESDs in parentheses. R-factors (%)†: R_{WP} = 11.0, R_P = 8.9, R_{NUC} = 9.0, R_{EX} = 3.3. Cell parameters: a = 10.4715(4) Å, b = 9.5158(3) Å, c = 7.1446(2) Å, β = 106.268(2)°.

Atom	Symmetry position	Fractional Coordinates			B_{iso} (Å^2)
		x	y	z	
Mn(1)	4(h)	0	0.1815(8)	½	0.11(5)
Mn(2)	4(i)	0.7972(8)	0	0.1410(12)	0.11(5)
Mo(1)	4(g)	0	0.2547(4)	0	0.11(5)
Mo(2)	4(i)	0.2692(4)	0	0.4087(6)	0.11(5)
O(1)	4(i)	0.3560(5)	½	0.4595(8)	0.52(4)
O(2)	4(i)	0.2044(5)	0	0.1553(8)	0.52(4)
O(3)	8(j)	0.1374(4)	0.3538(4)	0.1100(5)	0.52(4)
O(4)	8(j)	0.4582(3)	0.3465(4)	0.1937(5)	0.52(4)
O(5)	8(j)	0.3658(3)	0.1509(4)	0.4742(6)	0.52(4)

† The R-factors are defined in [5].

Table 2. Bond distances (Å) and Mn–O–Mn angles (deg) for α-$MnMoO_4$ from the refinement using 50 K D1A powder neutron diffraction data, with ESDs in parentheses.

Mn(1)–O(1)	(×2)	2.257(7)	Mo(1)–O(3)	(×2)	1.716(4)
Mn(1)–O(4)	(×2)	2.125(4)	Mo(1)–O(4)	(×2)	1.837(4)
Mn(1)–O(5)	(×2)	2.099(7)	Mo(2)–O(1)		1.816(8)
Mn(2)–O(1)		2.185(10)	Mo(2)–O(2)		1.746(7)
Mn(2)–O(2)		2.112(11)	Mo(2)–O(5)	(×2)	1.743(4)
Mn(2)–O(3)	(×2)	2.139(8)			
Mn(2)–O(4)	(×2)	2.182(7)			
Mn(1)–O(1)–Mn(1′)		99.8(3)	Mn(1)–O(4)–Mn(2)		100.8(3)
Mn(1)–O(1)–Mn(2)		96.7(2)			

The magnetic peaks observed below T_N were indexed on a magnetic supercell with $\boldsymbol{a}_m = \boldsymbol{a}$, $\boldsymbol{b}_m = \boldsymbol{b}$, $\boldsymbol{c}_m = 2\boldsymbol{c}$, where $\boldsymbol{a}$, $\boldsymbol{b}$, and $\boldsymbol{c}$ are the nuclear cell vectors, and the magnetic reflection conditions were $h + k = 2n + 1$; $l = 2n + 1$. An excellent fit to the magnetic peaks (R_{WP} = 6.6%, R_P = 4.8%, R_{NUC} = 6.5%, R_{MAG} = 3.7%) was obtained from the model shown in figure 7, which has C_P2/m' symmetry. Neighbouring Mn(1) and Mn(2) spins were constrained to be equal and parallel and to lie in the (010) plane. No evidence was found for a canted or non-collinear magnetic structure. At 2 K the refined magnetic components parallel to $\boldsymbol{a}_m$ and $\boldsymbol{c}_m$ were 2.88(14) and 4.62(8) μ_B, respectively, corresponding to a resultant moment of 4.71(3) μ_B close to the [101] direction of the magnetic cell. No change in the magnetic structure was observed between 2 K and T_N other than a typical Brillouin temperature-dependence of the magnetic moment.

The degree of covalency in the bonding about an octahedrally coordinated d^5 cation can be estimated from the observed moment (S) using equation (1)

$$S/S_0 = 1 - 1.2(f_\sigma + 2f_\pi + f_s) \tag{1}$$

which derives from molecular orbital theory [13]. S_0 is the free-ion spin corrected for zero-point deviation and the f-terms are the fractions of unpaired spin transferred to a

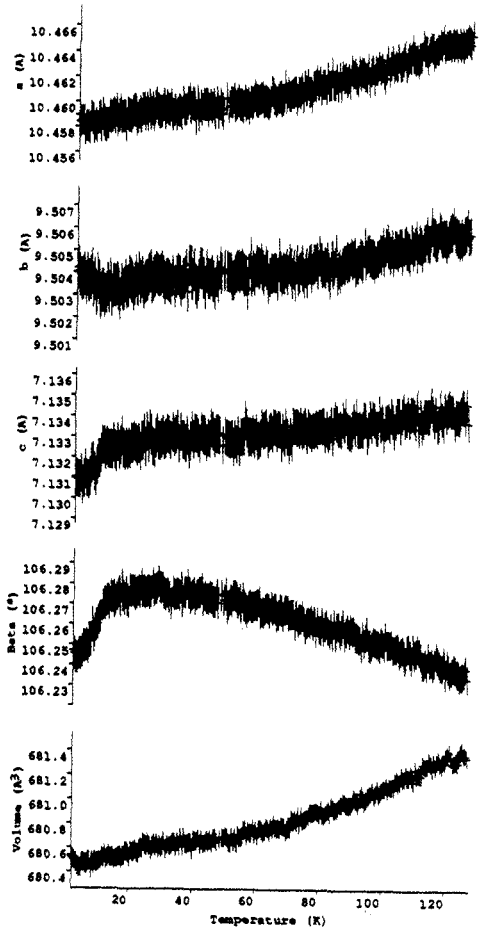

Figure 4. Temperature dependences of (from top to bottom) the refined cell parameters a, b, c, β, and the cell volume of α-$MnMoO_4$ between 2 and 127 K. The error bars correspond to one ESD.

ligand pσ, pπ, or s orbital. Assuming the zero-point spin deviation to be the same as that in MnO (2.76% [14]), this gives the sum of covalent interactions in α-$MnMoO_4$ to be $f_\sigma + 2f_\pi - f_s = 2.6(12)\%$.

4. Discussion

This neutron diffraction study shows that α-$MnMoO_4$ undergoes a structural phase transition at $T_s = 79.1(2)$ K, which reduces the symmetry from $C2/m$ to $P2/m$ (or lower), and a three-dimensional antiferromagnetic transition at $T_N = 10.7(2)$ K, in fair agreement with susceptibility results [9]. The 50 K D1A pattern does not have sufficient resolution or peak-to-background ratios for the $h + k = 2n + 1$ reflections to enable the low-symmetry structure to be determined. However, the refinement of individual temperature factors in $C2/m$ suggests that the transition may involve displacements of Mo(2), O(2), and O(5) so as to make the molybdate groups centred in the $y = 0$ and $y = \frac{1}{2}$ planes inequivalent. Fitting this profile in $C2/m$ gives results (tables 1 and 2) that are in excellent agreement with those at room temperature [8], and neither the cell parameters in figure 4 nor any of the fractional coordinates show any discontinuity at

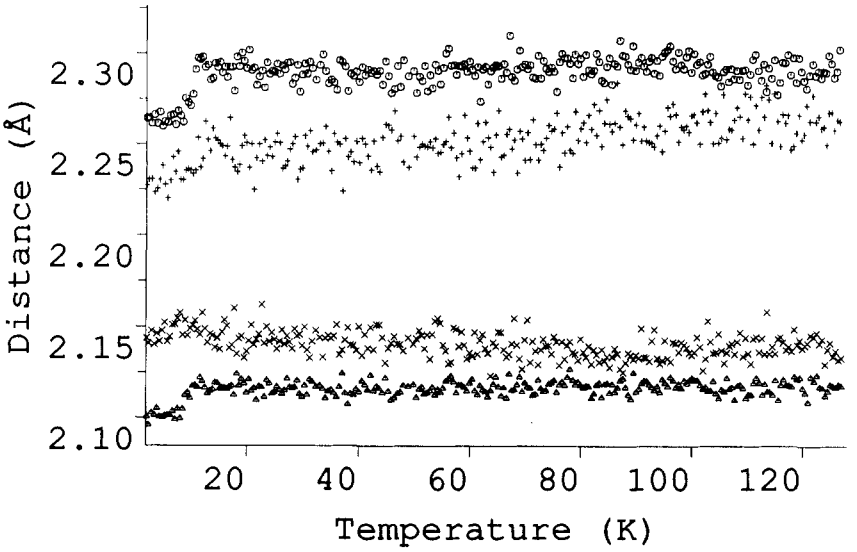

Figure 5. Temperature variations of (from top to bottom) the Mn(1)–O(1), Mn(2)–O(1), Mn(2)–O(4), and Mn(1)–O(4) bond distances (ESDs ~ 0.01 Å) in α-$MnMoO_4$ between 2 and 127 K.

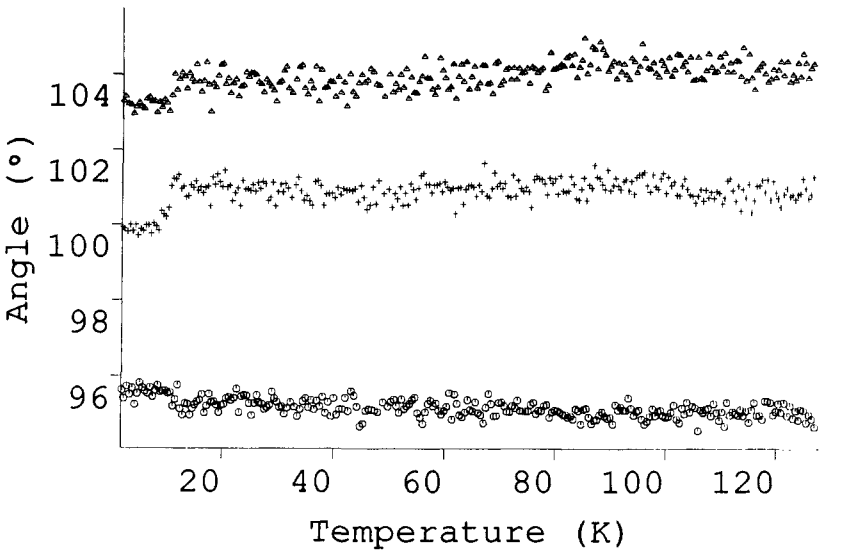

Figure 6. Temperature variations of (from top to bottom) the Mn(1)–O(4)–Mn(2), Mn(1)–O(1)–Mn(1), and Mn(1)–O(1)–Mn(2) angles (ESDs ~ 1°) in α-$MnMoO_4$ between 2 and 127 K.

T_s, indicating that this distortion is extremely small. Hence, the refinements in $C2/m$ should provide structural descriptions that are adequate over the range of temperatures studied; single-crystal neutron diffraction will be required to determine the true structure below T_s.

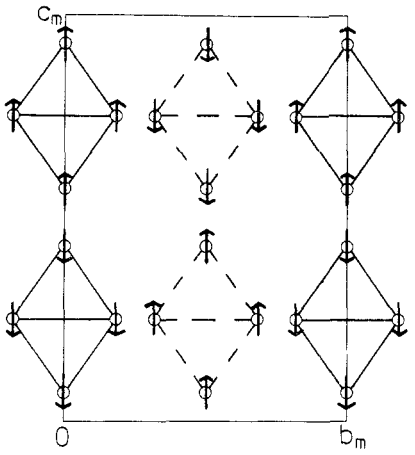

Figure 7. (100) view of the magnetic cell of α-$MnMoO_4$. Mn^{2+} positions are shown by circles and the magnetic moments are collinear and close to [101]. The intracluster magnetic interactions are also shown; full (broken) lines correspond to clusters centred in the $x = 0$ ($\frac{1}{2}$) planes.

The parallel alignment of the four spins within each Mn_4O_{16} cluster shows that the interactions between Mn^{2+} spins are ferromagnetic. This is very unusual for superexchange through the bridge 1, as the coupling is predicted to be anti-

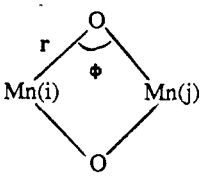

1

ferromagnetic from the Goodenough–Kanamori rules [15], and this has been verified for many Mn $(X)_2Mn$ bridges. For example, $MnSO_4$ [16], α-$MnSeO_4$ [17], and β-$MnSeO_4$ [18] all contain infinite one-dimensional chains of edge-sharing octahedra with r and φ values similar to those in α-$MnMoO_4$, and in all three cases the coupling along the chains is antiferromagnetic. The cause of the present ferromagnetic coupling may therefore result from the linking of $Mn(O)_2Mn$ bridges in the cluster, shown schematically in 2.

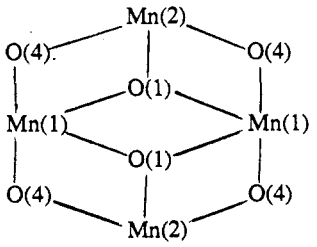

2

The magnetic exchange constant for the interaction shown in contains both antiferromagnetic (kinetic) and ferromagnetic (potential) contributions [19] both of which are enhanced through covalency in the Mn–O bonds. For a 90° d^5–d^5 inter-

action the most significant ferromagnetic contribution arises from σ-overlap of orthogonal O^{2-}:$2p_\sigma(x)$ and $2p_\pi(y)$ orbitals with Mn^{2+}:e_g orbitals. Intra-atomic exchange between the spins delocalised onto the anion stabilises the ferromagnetic state. A possible enhancement of this interaction in α-$MnMoO_4$ arises from the fact that three 90° pathways take place through O(1) (see ②) which allows spin to be transferred into the three orthogonal O^{2-}:$2p_\sigma(x)$, $2p_\pi(y)$, and $2p_\sigma(z)$ orbitals. This will result in a greater intra-atomic exchange than in ① as the total exchange increases with the number of unpaired spins, n as $n(n-1)$, so that the potential exchange may outweigh the kinetic terms. Hence, the ferromagnetic order in the Mn_4O_{16} clusters may best be described as resulting from a 90, 90, 90° Mn–O(Mn)–Mn interaction rather than several 90° Mn–O–Mn interactions. It is interesting to note that a d^5-cation material with a network of X intersecting 90° M–X–M bridges might order ferromagnetically with a large saturation moment, provided no other (antiferromagnetic) pathways were active.

The weak intercluster superexchange interactions that take place through the molybdate groups in α-$MnMoO_4$ are antiferromagnetic, as observed in other molybdates [20, 21], and result in overall antiferromagnetism with neighbouring clusters having opposite spin directions as shown in figure 7. The diffuse scattering observed at $2\theta = 15°$ in the D1B profiles (figure 3) at temperatures around T_N indicates that some short-range magnetic order also occurs. This may reflect significant ferromagnetic alignments within the clusters before the long-range antiferromagnetic order sets in, as the former interactions are expected to be much stronger than the latter. The sum of covalent interactions in α-$MnMoO_4$ of 2.6(12)% may be compared with those derived from published results for $MnSO_4$ (1% [16]), $Fe_2(MoO_4)_3$ (9.1(12)% [20]), and $Fe_2(SO_4)_3$ (6.1(33)% [22]). These results demonstrate that ligand (XO_4^{n-}) to metal (M^{m+}) charge transfer increases with the increasing charge on M and the decreasing electronegativity of X.

Figure 4 shows that a deformation of the unit cell takes place at T_N, although there is no decrease in volume, and discontinuities in some fractional coordinates were also observed. These data were used to derive the variations of the distances and angles of the bonds involved in the superexchange pathways in ②. The results in figures 5 and 6 reveal contractions of 0.02 Å in three of the four Mn–O bonds between T_N and 2 K, and decreases of 1° in the Mn(1)–O(1)–Mn(1) and Mn(1)–O(4)–Mn(2) angles. Although these quantities may be in error due to the assumptions made in the structure refinements, they are generally consistent with the magnetic order, as the structure will tend to undergo an exchange-strictive distortion below T_N so as to increase the strength of the dominant ferromagnetic interactions within the clusters by decreasing r and decreasing φ towards 90°. The slight increase observed in the Mn(1)–O(1)–Mn(2) angle may result from the strains imposed by the other distortions.

The results indicate that detailed magneto-structural correlations may be obtained by following the structural changes that accompany magnetic order. Although the refinements are of low precision due to the limited range of data and ignorance of the low-temperature structure of α-$MnMoO_4$, they are sufficient to reveal details of the exchange-strictive distortions of this moderately complex framework. These distortions may also be used to estimate the sign and approximate values of the magnetic exchange constants [7]. Continuing developments in time-of-flight neutron spectrometers and constant wavelength x-ray and neutron diffractometers with position-sensitive detectors will enable such studies to be performed with greater precision and for more complex materials in the future.

Acknowledgments

The author thanks Drs A Hewat and J Pannetier for assistance with the collection of neutron data, SERC for providing neutron facilities, and Christ Church, Oxford for a Junior Research Fellowship.

References

[1] Attfield J P, Battle P D and Cheetham A K 1985 *J. Solid State Chem.* **57** 357
[2] Battle P D, Gibb T C, Hu G, Munro D C and Attfield J P 1986 *J. Solid State Chem.* **65** 343
[3] Attfield J P, Cheetham A K, Johnson D C and Torardi C C 1987 *Inorg. Chem.* **26** 3379
[4] Attfield J P, Battle P D, Cheetham A K and Johnson D C 1989 *Inorg. Chem.* **28** 1207
[5] Rietveld H M 1969 *J. Appl. Crystallogr.* **2** 65
[6] Rodriguez-Carvajal J, Martinez J L, Pannetier J and Seaz-Puche R 1988 *Phys. Rev.* B **38** 7148
[7] Attfield J P 1989 *J. Phys.: Condens. Matter* **1** 7045
[8] Abrahams S C and Reddy J M 1965 *J. Chem. Phys.* **43** 2533
[9] Van Uitert L G, Sherwood R C, Williams H J, Rubin J J and Bonner W A 1964 *J. Phys. Chem. Solids* **25** 1447
[10] Cox D E 1984 *Acta Crystallogr.* A **40** C369
[11] Sears V F 1984 Thermal neutron scattering lengths and cross sections for condensed matter research *Chalk River Nuclear Laboratory Internal Report* AECL-8490
[12] Freeman A J and Watson R E 1961 *Acta Crystallogr.* **14** 231
[13] Tofield B C 1975 *Struct. Bonding* **21**
[14] Jacobson A J, Tofield B C and Fender B E F 1973 *J. Phys. C: Solid State Phys.* **6** 1615
[15] Goodenough J B 1963 *Magnetism and the Chemical Bond* (New York: Wiley)
[16] Will G, Frazer B C, Shirane G, Cox D E and Brown P J 1965 *Phys. Rev.* **140** A2139
[17] Kirfel A and Will G 1973 *Int. J. Magn.* **5** 197
[18] Fuess H and Will G 1968 *J. Appl. Phys.* **39** 628
[19] Anderson P W 1963 *Solid State Physics* vol 14 (New York: Academic) p 99
[20] Battle P D, Cheetham A K, Long G L and Longworth G 1982 *Inorg. Chem.* **21** 4223
[21] Battle P D, Cheetham A K, Harrison W T A, Pollard N J and Faber J 1985 *J. Solid State Chem.* **58** 221
[22] Long G L, Longworth G, Battle P D, Cheetham A K, Thundathil R V and Beveridge D 1979 *Inorg. Chem.* **18** 624